Biochimica et Biophysica Acta 1832 (2013) 553–564

Contents lists available at SciVerse ScienceDirect

Biochimica et Biophysica Acta

journal homepage: www.elsevier.com/locate/bbadis

Loss of connexin43 expression in Ewing's sarcoma cells favors the development of the primary tumor and the associated bone osteolysis ☆

Julie Talbot [a,b,c,d,e], Régis Brion [a,b,c,d,e], Gaëlle Picarda [a,b,c,d,e], Jérome Amiaud [a,b,c,d,e], Julie Chesneau [a,b,c,d,e], Gwenola Bougras [a,b,c,d,e], Verena Stresing [a,b,c,d,e], Franck Tirode [f], Dominique Heymann [a,b,c,d,e], Françoise Redini [a,b,c,d,e], Franck Verrecchia [a,b,c,d,e,*]

[a] LUNAM Université, France
[b] INSERM, UMR 957, Nantes, France
[c] Université de Nantes, Laboratoire de Physiopathologie de la Résorption Osseuse et Thérapie des Tumeurs Osseuses Primitives, Nantes, France
[d] CHU Hôtel Dieu, Nantes, France
[e] Equipe labellisée Ligue contre le Cancer 2012, Nantes, France
[f] Institut Curie, INSERM U830, Paris, France

ARTICLE INFO

Article history:
Received 20 August 2012
Received in revised form 13 December 2012
Accepted 2 January 2013
Available online 9 January 2013

Keywords:
Connexin43
Ewing's sarcoma
EWS–FLI1
Osteolysis
Tumor growth

ABSTRACT

Ewing's sarcoma (ES) is a primary bone tumor characterized by a chromosomic translocation between the EWS gene and a member of the ETS gene family, mainly FLI1, which leads to an aberrant transcription factor EWS–FLI1 that promotes tumorigenicity. Gap junctions are intercellular channels composed of transmembrane proteins (connexin: Cx), that allow direct intercellular communication between adjacent cells. Numerous studies have shown that tumorigenesis may be associated with a loss of gap junctional intercellular communication (GJIC). Loss of Cx43 expression was observed at the protein and mRNA levels in ES cell lines compared to those measured in human mesenchymal stem cells. A673 ES cells stably transfected with an shRNA targeting EWS–FLI1 showed an increase in Cx43 expression (at the mRNA, protein and transcriptional levels) and GJIC. In an osteolytic murine model of ES, the overexpression of Cx43 in ES cells dramatically reduced tumor growth, leading to a significant increase in animal survival. In vitro assays showed that Cx43 overexpression increases the p27 level with an associated marked decrease of Rb phosphorylation, consistent with the observed blockade of the cell cycle in G0/G1 phase. In addition, the bone microarchitectural parameters, assessed by micro-CT analysis, showed an increased bone volume when Cx43 expression was enhanced. Histological analysis demonstrated that the overexpression of Cx43 in ES tumor cells inhibits osteoclast activity and therefore bone resorption. Our study demonstrated that the loss of Cx43 expression in ES cells plays a crucial role in the development of the primary tumor and the associated bone osteolysis.

1. Introduction

Ewing's sarcoma (ES) is the second most frequent pediatric bone cancer after osteosarcoma. It is a rare, aggressive, poorly differentiated tumor of bone and soft tissue which occurs primarily in children, adolescents and young adults [1–3]. ES is characterized by a rapid proliferation of tumor cells with small round nuclei that causes extensive and rapidly progressive bone destruction [4]. ES is a classic example of a malignancy driven by a fusion oncogene, 85% of ES tumor specimens harboring the t(11;22)(q24;q12) chromosomal rearrangement [5]. The resultant fusion transcript EWS–FLI1 is formed by the N-terminal part of the EWS protein linking to the DNA-binding domain (ETS domain) of the FLI1 transcription factor [6]. FLI1 possesses carcinogenic properties of cell cycle induction, aberrant transcription and promotion of cell survival when associated with EWS [7]. Alternative rarer translocations are known such as, EWS/ERG occurs in approximately 10% of cases, EWS/ETV, EWS/EIAF and EWS/FEV each in <1% of cases. Although the cell origin of ES remains unknown, there is a growing body of evidence that suggests ES is derived from human mesenchymal stem cells (hMSC). Indeed, strong arguments indicate that the fusion gene EWS-FLI1 may induce the transformation of hMSC into ES cells [8].

Connexins, the structural proteins of gap junctions, are a family of transmembrane proteins that oligomerize into hemichannels containing six connexin subunits [9]. Upon reaching the cell surface, two hemichannels pair to complete an intercellular gap junction channel, which directly links the cytoplasm of neighboring cells and mediate the exchange of low-molecular-mass molecules (<1000 Da), including

☆ Financial support: INSERM; Région Pays de la Loire (R09010NN-REGIONPDL); Ligue contre le Cancer (Equipe labellisée 2012).

* Corresponding author at: INSERM U957, Faculté de Médecine, 1 rue Gaston Veil, 44000 Nantes, France. Tel.: +33 240412842; fax: +33 240412860.
E-mail address: franck.verrecchia@inserm.fr (F. Verrecchia).

0925-4439/$ – see front matter © 2013 Elsevier B.V. All rights reserved.
http://dx.doi.org/10.1016/j.bbadis.2013.01.001

cAMP, inositol trisphosphate, and Ca^{2+} [10]. The permeability of gap junctions is finely regulated at the transcriptional [11,12] and posttranslational level via cycles of connexin phosphorylation [13], intracellular Ca^{2+} or H^+ concentrations [14,15] (for reviews, see Refs. [16–18]). A critical role in the progression of a variety of tumors has been attributed to gap junction intercellular communication (GJIC) [19,20]. Reduced or loss of gap junctional activity through different mechanisms including reduced expression has been implicated in various human cancers [21]. The crucial role of altered GJIC in tumor progression was further demonstrated by the exogenous expression of connexins in gap junction-deficient cell lines, which was shown to restore functional communication and to delay tumor growth [22,23]. The number of possible mechanisms responsible for connexin-mediated tumor suppression has grown with insights into the possible functional roles of hemichannels [24], cross-talk between gap junctions and other adhesion-based junctional complexes [25] and the discovery of novel connexin-binding proteins [26]. Thus, increasing evidence suggests that GJ-independent mechanisms are also involved in connexin-mediated tumor suppression [20,21].

Despite many studies having demonstrated the importance of connexin43 (Cx43), the most abundant connexin in bone cells, for bone development and turnover during the last decade [27], little is currently known about GJIC and Cx43 in primary bone tumors. In this report, we analyzed the specific role of Cx43-driven GJIC in ES tumor growth. Using a combination of in vitro and in vivo experimental approaches, we demonstrated: i) a lack of Cx43 gene expression in ES cells, ii) that the expression level of Cx43 is associated with that of EWS–FLI1, iii) that Cx43 inhibits ES tumor growth via modulation of cell proliferation, and iv) Cx43 reduces tumor cell-driven osteoclast activity.

2. Materials and methods

2.1. Cell cultures

Human ES cells were cultured in DMEM (Dulbecco's Modified Eagle's Medium, Lonza, Basel, Switzerland) or RPMI (Roswell Park Memorial Institute, Lonza) supplemented with 10% fetal bovine serum (FBS; Hyclone Perbio, Bezons, France). A673 ES cells stably transfected with an inducible shRNA against EWS–FLI1 were treated with doxycycline (1 μg/ml) to induce shRNA expression (A673-1c cells) [8]. Bone marrow, harvested by iliac crest aspiration from donors (age = 46 ± 12; range = 36–67), were obtained from the "Etablissement Français du Sang" with informed consent and ethical approval from the Nantes University Hospital Ethics Committee. hMSCs were cultured in DMEM, 10% FBS, 1 ng/ml basic fibroblast growth factor (R&D systems, Lille, France). Adherent cells were characterized by flow cytometry ($CD45^-$, $CD34^-$, $CD105^+$, $CD73^+$and $CD90^+$, purity ≥ 99%) prior to further experiments.

All in vitro experiments were made with identical number of cells at the same density.

2.2. Western blot analysis

Cells were lysed in a lysis buffer (SDS 1%, Tris pH 7.4 10 mM, sodium orthovanadate 1 mM) and protein concentration was determined by BCA kit (Sigma, St Quentin-Fallavier, France). 10 μg of total protein extracts in Laemmli buffer (62.5 mM Tris–HCl, pH 6.8, 2% SDS, 10% glycerol, 5% 2-mercaptoethanol, 0.001% bromophenol blue) were separated by SDS-polyacrylamide gel electrophoresis, and transferred to Immobilon-P membranes (Millipore, Billerica, MA, USA). Membranes were immunoblotted with mouse monoclonal anti-Connexin43 (dilution 1/1000, Sigma), rabbit polyclonal anti-Fli1 (dilution 1/1000, Santa Cruz Biotechnology, CA, USA), mouse monoclonal anti-GAPDH (dilution 1/2000, Abcam, Paris, France), or rabbit polyclonal anti-β-actin (dilution 1/10,000, Sigma) antibodies. Antibody binding was visualized with the enhanced chemiluminescence system (SuperSignal West Pico Chemiluminescent Substrate, ThermoSientific, Illkirch, France). For quantification, luminescence was detected with a Charge Couple Device (CCD) camera and analyzed using the GeneTools program (Syngene, Cambridge, United Kingdom). To specifically evaluate the phosphorylation status of Cx43, cells were lysed in RIPA buffer (10 mM Tris pH8, 1 mM EDTA, 150 mM NaCl, 1% NP40, 0.1% SDS) containing a cocktail of protease and phosphatase inhibitors (1 mM sodium orthovanadate (Na_2VO_4), 1 mM phenylmethylsulforyl fluoride (PMSF), 10 mM sodium fluoride (NaF), 10 mM N-ethylmaleimide (NEM), 2 μg/ml leupeptin and 1 μg/ml pepstatine) at 4 °C and were sonicated twice for 30 s. 50 μg of total protein were then separated by SDS-polyacrylamide gel electrophoresis.

2.3. Cx43 immunostaining

Cells were cultured in plastic chamber microscope slides (Millicell EZ Slide, Millipore, Billerica, MA, USA), fixed in 4% paraformaldehyde for 10 min at room temperature, and permeabilized in 0.5% saponin/PBS. Cells were incubated with a primary antibody (mouse monoclonal anti-Cx43, Sigma) at a 1:100 dilution for 2 h at room temperature and a secondary antibody (Alexa Fluor 647 nm goat anti-mouse IgG, Invitrogen, Carlsbad, CA, USA) at a 1:500 dilution for 1 h at room temperature. Slides were mounted with liquid Prolong Gold antifade reagent with Dapi (Molecular Probes) and observed under a confocal microscope (Nikon A1Rs 60× NA 1.4). All controls performed by omitting the primary antibody were negative.

2.4. Cell cycle analysis

Cells were incubated in serum-free medium during 12 h and then in medium supplemented with 10% serum. Cell cycle distribution was studied by flow cytometry (Cytomics FC500; Beckman Coulter, Villepinte, France) based on 2 N and 4 N DNA content (50 μg/ml propidium iodide) and analyzed by using DNA Cell Cycle Analysis Software (Phoenix FlowSystems, San Diego, CA, USA).

2.5. Real-time polymerase chain reaction

Total RNA was extracted using NucleoSpin®RNAII (Macherey Nagel, Duren, Germany). 1 μg of total RNA was used for first strand cDNA synthesis using ThermoScript RT-PCR System (Invitrogen). DNase I treatment (25 units, 15 min) of total RNA was performed to eliminate genomic contamination. Real-time PCR was performed with a Chromo4 instrument (Biorad, Richmond, CA, USA) using SYBR Green Supermix reagents (Biorad). Primer sequences are provided in Supplementary Table 1. Calibration curves with different amounts of cDNA were used to validate the primers according the MIQE guidelines [28].

2.6. Transient cell transfections, reporter assays and plasmid constructs

Transient cell transfections were performed with jetPEI™ (Polyplus-transfection, Illkirch, France). The phRLMLP-*Renilla* luciferase expression vector was cotransfected in every experiment to monitor transfection efficiencies. Luciferase activity was determined with the Dual-Luciferase reporter assay system (Promega, Charbonnieres, France). The *Cx43* promoter/gene reporter construct −2400Cx43-lux has been described previously [29]. The expression vector of the *Cx43* gene was generated by PCR using the Cx43-EGFP plasmid [30] as template and cloned inpcDNA3.1 vector.

2.7. Parachute assay

GJIC was determined by parachute assay, as previously described [31,32]. This method utilizes fluorescence-activated cell sorting (FACS) analysis to study intercellular dye transfer. Briefly, cell cultures were divided into "acceptor" and "donor" cell groups. Adherent

acceptor cells were loaded with DiI (Sigma), a nontransferable membrane dye for 1 h, and confluent donor cells were dyed with calcein-acetoxymethylester (calcein-AM; Sigma) for 45 min. After loading, cells were washed in PBS to remove the excess dye. Then, the calcein-AM-dyed cells were trypsinized and parachuted on the DiI-dyed acceptor cell layer at a cell ratio of 1/10 and incubated for 2 h at 37 °C to allow dye transfer via gap junctions. Dye coupling was analyzed using flow cytometry conducted with a FACS FC500 cytometer. For the analysis of results, gates were established on the day of each experiment using non-dyed cells, cells dyed with calcein-AM, and cells dyed with DiI. The quantification of dye transfer is explained in more detail in Supplementary Figure S1 legend.

2.8. Ewing's sarcoma model

Four-week-old female Rj:NMRI-nude mice (Elevages Janvier, Le Genest Saint Isle, France) were maintained under pathogen-free conditions at the Experimental Therapy Unit (Faculty of Medicine, Nantes, France) in accordance with the institutional guidelines of the French Ethical Committee (CEEA Pays de la Loire no.06; CEEA-2010-23) and under the supervision of authorized investigators. The mice were anesthetized by inhalation of an isoflurane/air mixture (1.5%, 1 L/min) before receiving an intramuscular injection of $2 \cdot 10^6$ TC71 or A673 cells in close proximity to the tibia, leading to a rapidly growing tumor in soft tissue with secondary contiguous bone invasion. Tumors appeared at the injection site 8 days later. The tumor volume (V) was calculated from the measurement of two perpendicular diameters using a caliper, according to the following formula: $V = 0.5 \times L \times (S)^2$, in which L and S are, respectively, the largest and smallest perpendicular tumor diameters as previously described [33]. Mice were sacrificed when the tumor volume reached 3000 mm^3 for ethical reasons.

2.9. Micro-CT analysis

Analyses of bone microarchitecture were performed using the high-resolution X-ray micro-CT system for small-animal imaging SkyScan-1072 (SkyScan, Kartuizersweg, Belgium). Analyses were performed both on live and anesthetized animals [xylazine (Rompun®; Bayer)-ketamine (Imalgène®1000; Merial) 8% and 13%, respectively, in PBS; 100 μl/10 g], at different tumor volumes (500 and 1000 mm^3), and at necropsy (3000 mm^3). All tibiae/fibulae were scanned using the same parameters (pixel size 18 μm, 50 kV, 0.5-mm Al filter and 0.8° of rotation step). Three-dimensional reconstructions and analysis of bone parameters were performed using CTvol and CTan software (Skyscan).

2.10. Bone histology

After sacrifice, the tibiae were conserved and fixed in 10% buffered formaldehyde, decalcified (4% EDTA, 0.2% paraformaldehyde, pH 7.4), and embedded in paraffin. 3-μm sections of tumor-bearing tibiae were cut and stained for tartrate-resistant acid phosphatase (TRAP) to analyze osteoclast activity. Quantification of osteoclastic areas was done using ImageJ (National Institutes of Health, USA).

2.11. Immunohistochemistry

3-μm sections of tumor tissues (embedded in paraffin) were cut and stained for Ki-67, active caspase 3 and osterix, respectively, with monoclonal mouse anti-human Ki-67 (Dako, Trappes, France), rabbit polyclonal anti-active Caspase 3 (Abcam) or rabbit polyclonal anti-osterix (Abcam) antibodies. Immunodetection was performed using DAB Substrate-Chromogen (Dako) and counterstained with hematoxylin.

2.12. Statistical analysis

All analyses were performed using GraphPad Prism 4.0 software (GraphPad Software, La Jolla, CA, USA). In vitro experiments results were analyzed with the unpaired *t*-test and are given as mean ± SD. For in vivo experiments, results from groups overexpressing Cx43 were compared with control groups (Parental and Mock) using the ANOVA test followed by Dunnett's multiple comparison test and are given as mean ± SEM. Results with $p<0.05$ were considered significant.

3. Results

3.1. Loss of Cx43 gene expression in ES cells

To evaluate the Cx43 production in ES cells, Western-blot analysis was performed to compare Cx43 protein levels in seven ES cell lines with those measured in hMSC from five healthy donors. As shown in Fig. 1A, Cx43 protein levels were dramatically reduced in all tested ES cell lines (by approximately 80%) with regard to the mean level measured in hMSC. To determine whether this decrease occurred via modulation of the corresponding gene, *Cx43* mRNA steady-state levels were measured by qRT-PCR. As shown in Fig. 1B, the *Cx43* mRNA levels are dramatically reduced in ES cells. By contrast, the expression of *Cx45*, a connexin expressed by both hMSC and ES cells, was not significantly different in hMSC and ES cells (Fig. 1C).

The Cx43 localization was then examined by immunostaining (Fig. 1D). As previously described [34], Cx43 is expressed predominantly along regions of intimate cell-to-cell contact and also within regions of the cytoplasm in hMSC cells. In the region of intercellular contact, Cx43 has a high punctate distribution which is characteristic for GJ channels. In ES cells, such as RDES (Fig. 1D) or A673, TC32, EW24 and TC71 (not shown) cells, Cx43 expression is observed along regions of intimate cell-to-cell contact. A low expression of Cx43 is also observed within the cytoplasm in ES cells indicating that the localization of Cx43 is not fundamentally different between hMSC and ES cells.

To determine whether loss of Cx43 gene expression is associated with gap junctional intercellular communication changes, GJIC was quantified by FACS analysis using the parachute assay. As shown in Fig. 1E, a strong decrease (approximately 70%) of the transfer-ratio was measured in A673 ES cells compared to hMSCs cells, indicating that the loss of Cx43 gene expression in A673 cells is associated with a decrease in the ability of these cells to form functional channels. Similar results were obtained using other ES cells such as TC71, EW24, RDES and TC32 cells (not shown).

To exclude the hypothesis that a defect of Cx43 phosphorylation could explain the decrease in GJIC observed in ES cells, a Western-blot analysis under appropriate conditions was performed. As shown in Fig. 1F, the phosphorylated forms of Cx43 (P_1 and P_2 bands) were detected in both, hMSC and ES cells.

Together these results demonstrate that the decrease of GJIC in ES cells is mainly due to the loss of Cx43 expression rather than to a defect of Cx43 localization and/or phosphorylation.

3.2. EWS–FLI1 represses Cx43 gene expression

Given the crucial role played by EWS–FLI1 in ES tumor growth, we hypothesized that EWS–FLI1 may regulate Cx43 gene expression. To test this theory, A673 ES cells stably transfected with an inducible shRNA targeting EWS–FLI1 were treated with doxycycline to induce shRNA expression (A673-1c cells) [8]. As expected, the presence of doxycycline induced a decrease in EWS–FLI1 protein levels in a time-dependent manner (Fig. 2A). Interestingly, when EWS–FLI1 production was decreased, this caused a subsequent increase in Cx43 protein levels (Fig. 2A). A673-1c cells exhibited a 7-fold higher

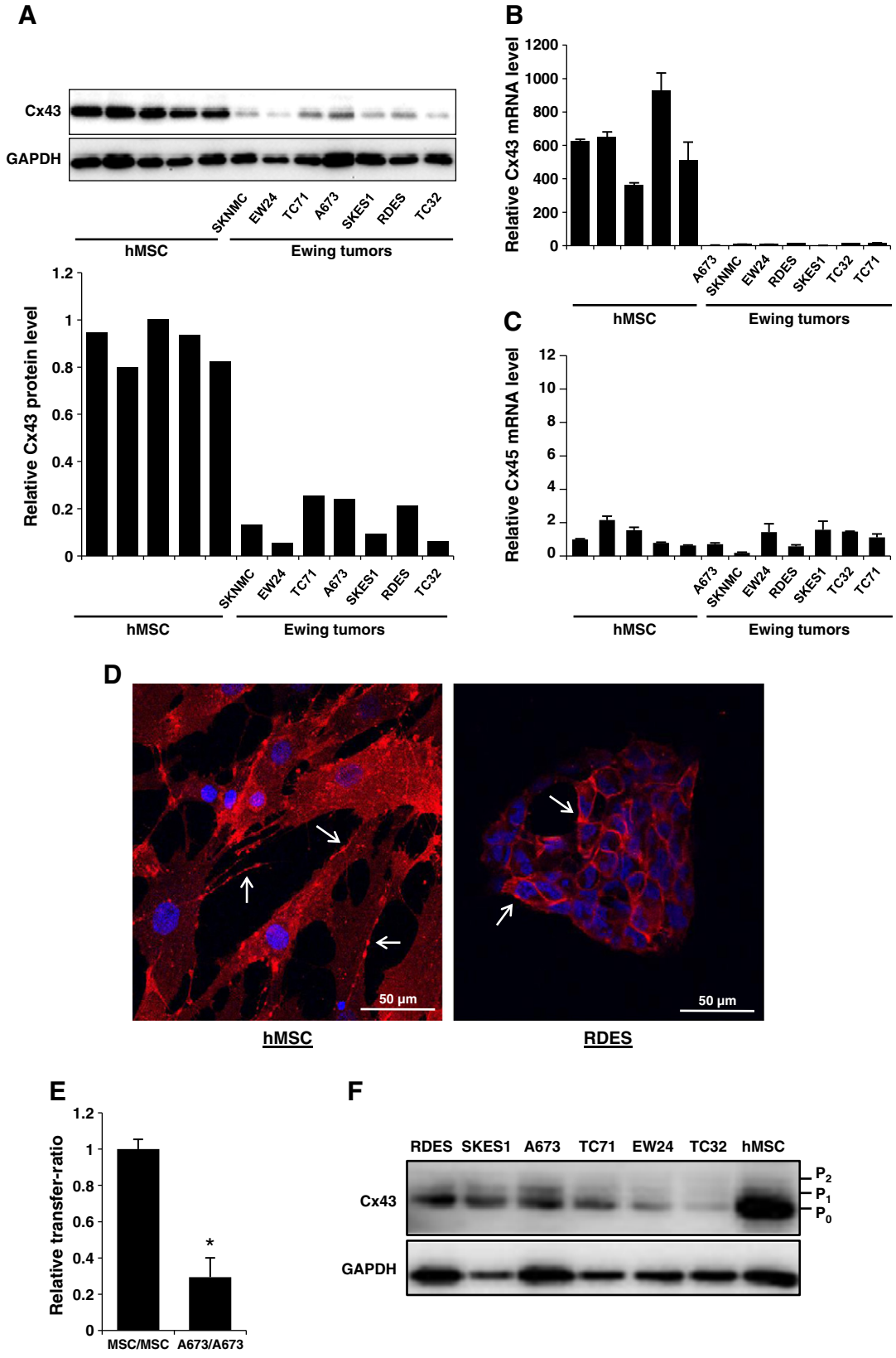

Fig. 1. Loss of Cx43 gene expression in ES cell lines (A) Cx43 production was detected by Western blot analysis of whole cell lysates of hMSC from five healthy donors and seven ES cell lines (upper panel). Specificity of the modulation was confirmed with an anti-GAPDH antibody (middle panel). The ratio of Cx43 to GAPDH is plotted from the values of one representative experiment of three experiments (lower panel). (B) *Cx43* mRNA steady-state levels in hMSC and ES cell lines were determined by qRT-PCR. Bars indicate mean ± SD of three independent experiments performed, each with duplicate samples. (C) *Cx45* mRNA steady-state levels in hMSC and ES cells were determined by qRT-PCR. Bars indicate mean ± SD of three independent experiments performed in duplicate. (D) Cultures of hMSC and ES cells were fixed, permeabilized and stained with a monoclonal antibody directed against Cx43 as detected by indirect immunofluorescence. Cx43 immunolocalization (red) and counterstaining of nuclei (dapi, blue) show high immunostaining at cell–cell boundaries (arrows) and a weak immunostaining within the cytoplasm both in hMSC and ES cells. Images represent one representative experiment of three experiments. (E) FACS analysis of parachute studies in hMSC and A673 ES cells. Histograms indicate mean ± SD of the relative transfer-ratio of calcein between cells measured in three independent experiments performed in duplicate (*$p<0.05$). (F) Phosphorylation status of Cx43 was evaluated by Western blot analysis of whole cell lysates of hMSC and ES cells (upper panel, P_1 and P_2 bands). Specificity of the modulation was confirmed with an anti-GAPDH antibody (lower panel).

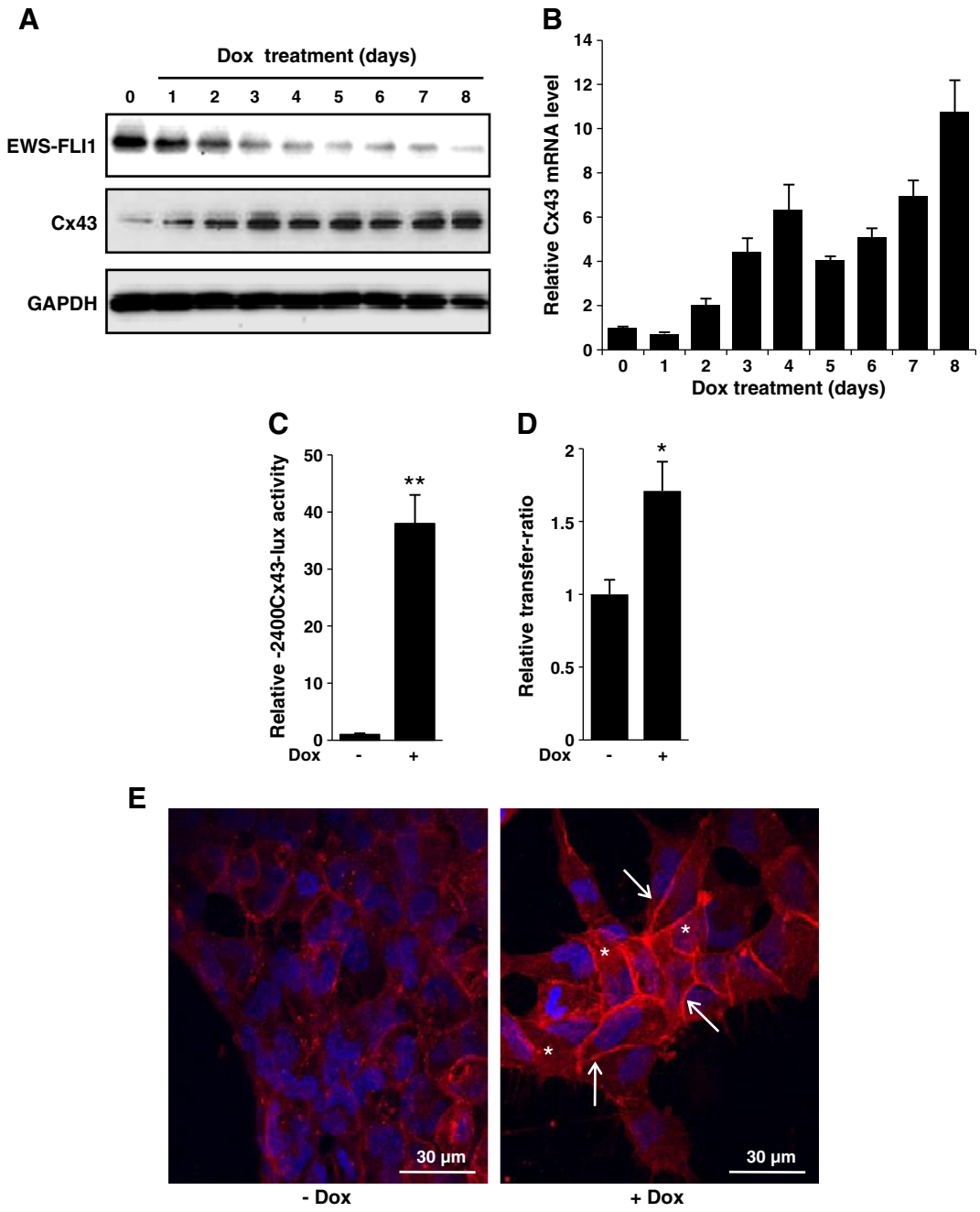

Fig. 2. Correlation between EWS–FLI1 and Cx43 gene expression. (A) A673-1c ES cells were treated with doxycycline (1 µg/ml) during 8 days. Cx43 and EWS–FLI1 production were detected by Western blot analysis. (B) A673-1c ES cells were treated with doxycycline (1 µg/ml) during 8 days. *Cx43* mRNA steady-state levels were determined by quantitative RT-PCR. Bars indicate mean ± SD of three independent experiments each performed in duplicate. (C) A673-1c ES cells were treated with doxycycline (1 µg/ml) during 3 days. After incubation, cell cultures were transfected with −2400Cx43-lux construct. 12 h after transfection, doxycycline was added and incubation continued for another 48 h. Bars indicate mean ± SD of three independent experiments each performed in duplicate (**$p<0.05$). (D) FACS analysis of calcein transfer in A673-1c cells treated with doxycycline (1 µg/ml) during 8 days compared to A673-1c untreated control cells. Histograms indicate mean ± SD of the relative transfer-ratio of calcein between cells measured in three independent experiments, carried out in duplicate (*$p<0.05$). (E) Cultures of A6731c were treated with doxycycline (1 µg/ml) for 8 days. After incubation, cells were fixed, permeabilized and stained with a monoclonal antibody directed against Cx43 as detected by indirect immunofluorescence. Images represent one representative experiment of three experiments.

production of Cx43 8 days after addition of doxycycline. To determine whether this increase in Cx43 protein production occurred via modulation of the corresponding gene, *Cx43* mRNA steady-state levels were measured by qRT-PCR. As shown in Fig. 2B, Cx43 expression was induced under doxycycline treatment. At day 2, 4 and 8 after addition of doxycycline, A673-1c cells respectively exhibited 2-, 6- and 10-fold higher *Cx43* mRNA steady state levels. To determine whether this effect of EWS–FLI1 on *Cx43* gene expression takes place at the transcriptional level, transient cell transfections were performed with the *Cx43* promoter/gene reporter construct −2400Cx43-lux. Doxycycline stimulation induced a 38-fold transactivation of the *Cx43* promoter (Fig. 2C). To determine whether the increase of *Cx43* gene expression in A673-1c under doxycycline stimulation is associated with gap junctional intercellular communication changes, GJIC was quantified by FACS analysis using the parachute assay. Doxycycline-induced Cx43 protein expression (Fig. 2A) significantly enhanced GJIC 8 days after addition of doxycycline (Fig. 2D).

Finally, Cx43 localization was examined by immunostaining. As shown in Fig. 2E (left panel) Cx43 is expressed predominantly along regions of intimate cell-to-cell contact and weakly within regions of the cytoplasm in absence of doxycycline. As illustrated in Fig. 2E (right panel), 8 days after treatment with doxycycline the increase in Cx43 expression measured using Western blot analysis (Fig. 2A) was both detected in the region of intercellular contact (Fig. 2E arrows) and within the cytoplasm (Fig. 2E asterisk). We can speculate that the low increase of GJIC (1.7 fold, Fig. 2D) under doxycycline treatment compared with the high increase in protein production (7-fold, Fig 2A) was mainly due to the fact that Cx43 expressed within the cytoplasm does not form functional intercellular channels.

Together, these results demonstrated that EWS–FLI1 represses *Cx43* gene expression and also the cell–cell communication between ES cells.

3.3. Overexpression of Cx43 in TC71 and A673 ES cell lines dramatically inhibits in vivo tumor growth

Since a reduced GJIC activity has been implicated in the development of various human cancers, we hypothesized that the decrease of *Cx43* gene expression observed in ES cells plays a role in ES tumor growth. Since we observed a loss of Cx43 gene expression in ES cells, a gain of function approach instead of a loss of function was used to test this hypothesis.

We stably transfected two human ES cell lines (TC71 and A673) with *Cx43* cDNA to examine this issue. Clones were generated, selected and analyzed in comparison with parental cell lines (P) and mock-transfected cells (M) for their Cx43 expression. To avoid the phenotypic artifacts that may result from the selection and propagation of individual clones derived from single transfected cells, a cell pool was generated. This pool, composed of cells from fifteen positive clones, was analyzed in comparison with parental cells and a pool of mock-transfected cells for their Cx43 mRNA and protein levels. Both Cx43–TC71 and Cx43–A673 cells expressed significantly higher levels of Cx43 mRNA (Fig. 3A) and protein (Fig. 3B) compared to parental and mock-transfected cells. Of note, the expression level of Cx45 is not modified after overexpression of Cx43 (not shown). In addition, we examined whether increased Cx43 expression in TC71 and A673 cells may affect their GJIC. In contrast to the low transfer-ratio measured in parental and mock-transfected cells, a significant increase in GJIC was observed in Cx43 overexpressing cells indicating that these cells were coupled forming interconnecting networks where they were able to communicate (Fig. 3C).

Next, a preclinical experimental model of ES induced by paratibial injection of either TC71 (Fig. 4) or A673 (Supplementary Fig. S2) ES cells was developed. Cx43 overexpression dramatically inhibited tumor growth in both TC71 and A673 injected mice (Fig. 4 and Supplementary Fig. S2). While 100% of mice injected with parental TC71 and 87.5% of mice receiving mock-transfected cells developed tumor volumes of $\geq$1000 mm^3 17 days after injection, only 25% of mice injected with Cx43-transfected cells developed a tumor volume of $\geq$1000 mm^3 (Fig. 4A). The mean tumor sizes at day 17 were respectively 2384$\pm$293 mm^3 and 2219$\pm$331 mm^3 in mice injected with parental and mock-transfected TC71 cells, whereas the mean tumor size in mice injected with the Cx43-transfected cells was 995$\pm$233 mm^3 (mean$\pm$SEM, $p<0.001$; Fig. 4B). Similar results were obtained in the A673 experimental model (Supplementary Fig. S2). The reduced mean tumor sizes indicated that Cx43 overexpression slowed tumor growth in both, the TC71 and A673 model by 55% ($p<0.05$) compared with control mice. Consequently, Cx43 overexpression increased animal survival by 70% ($p<0.05$) and 50% ($p<0.01$), respectively, in the TC71 (Fig. 4C) and A673 (Supplementary Fig. S2C) model compared with control animals.

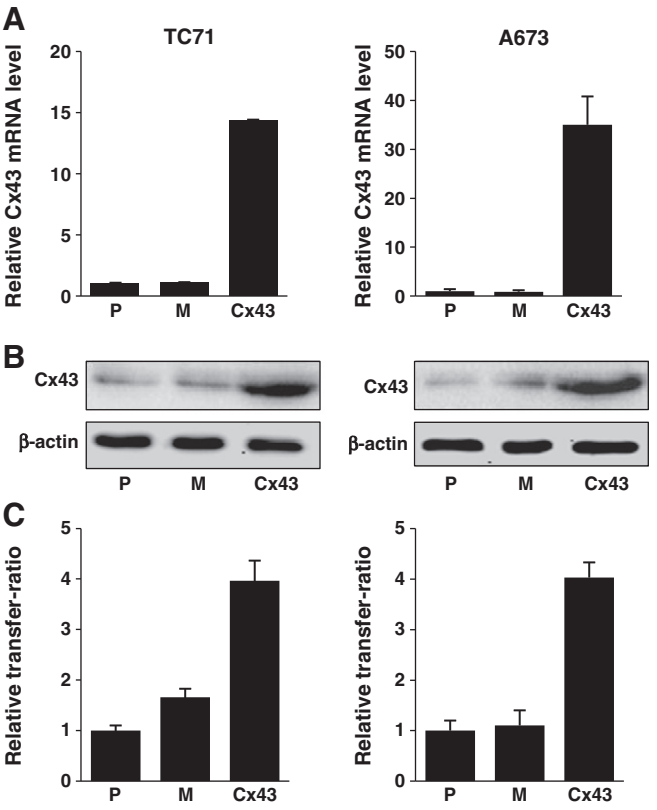

Fig. 3. Overexpression of Cx43 in TC71 and A673 ES cell lines. (A) *Cx43* mRNA steady-state levels in TC71 or A673 ES cells (parental (P), mock- (M), Cx43-transfected (Cx43)) were determined by quantitative RT-PCR. (B) Cx43 production in TC71 and A673 ES cell were determined by Western blot. (C) FACS analysis of parachute studies in TC71 and A673 ES cells. Histograms indicate mean$\pm$SD of the relative transfer-ratio of calcein between cells measured in three independent experiments performed, each with duplicate samples.

Tumors excised from sacrificed animals were then assessed for proliferation and apoptosis by immunohistochemical staining for Ki-67 and caspase-3, respectively. Staining for Ki-67 positive cells revealed that Cx43 overexpression resulted in a significant inhibition of cell proliferation in both ES experimental models (Fig. 5A), which is consistent with the smaller size of the Cx43 tumors. The mean number of Ki-67 positive cells counted by microscopy ($\times$20) in six random fields was 31$\pm$0.8 and 33$\pm$1.8, respectively, in tumors from mice injected with parental and mock-transfected TC71 cells, whereas this number was 20$\pm$1.4 in Cx43-expressing tumors (***$p<0.01$; Fig. 5A). Contrarily, staining for caspase-3 positive cells revealed no significant differences between the groups (data not shown) suggesting that the effect of Cx43 tumor growth is mainly due to inhibition of tumor cell proliferation rather than induction of tumor cell death.

To understand the mechanisms underlying the effect of Cx43 on cell proliferation, we carried out several in vitro experiments. First, a cell growth curve assay demonstrated that Cx43-transfected TC71 or A673 cells display a reduced proliferation rate (50% lower at day 7) compared to parental or mock-transfected cells (***$p<0.01$; Fig. 5B). Next, we performed flow cytometry of parental, mock- and Cx43-transfected TC71 and A673 cells to assess DNA content after 24 h of culture growth. Cx43 overexpression resulted in cell cycle arrest in G0/G1 phase (Fig. 5C), as demonstrated by a 50% increase in the number of cells in G0/G1 phase in Cx43-transfected cells compared with parental or mock-transfected cells in TC71 ES cells. Western blot analysis was then used to examine which DNA check points in cells were involved in mediating cell cycle arrest. As shown in Fig. 5D, Cx43 overexpression increased p27 levels with an

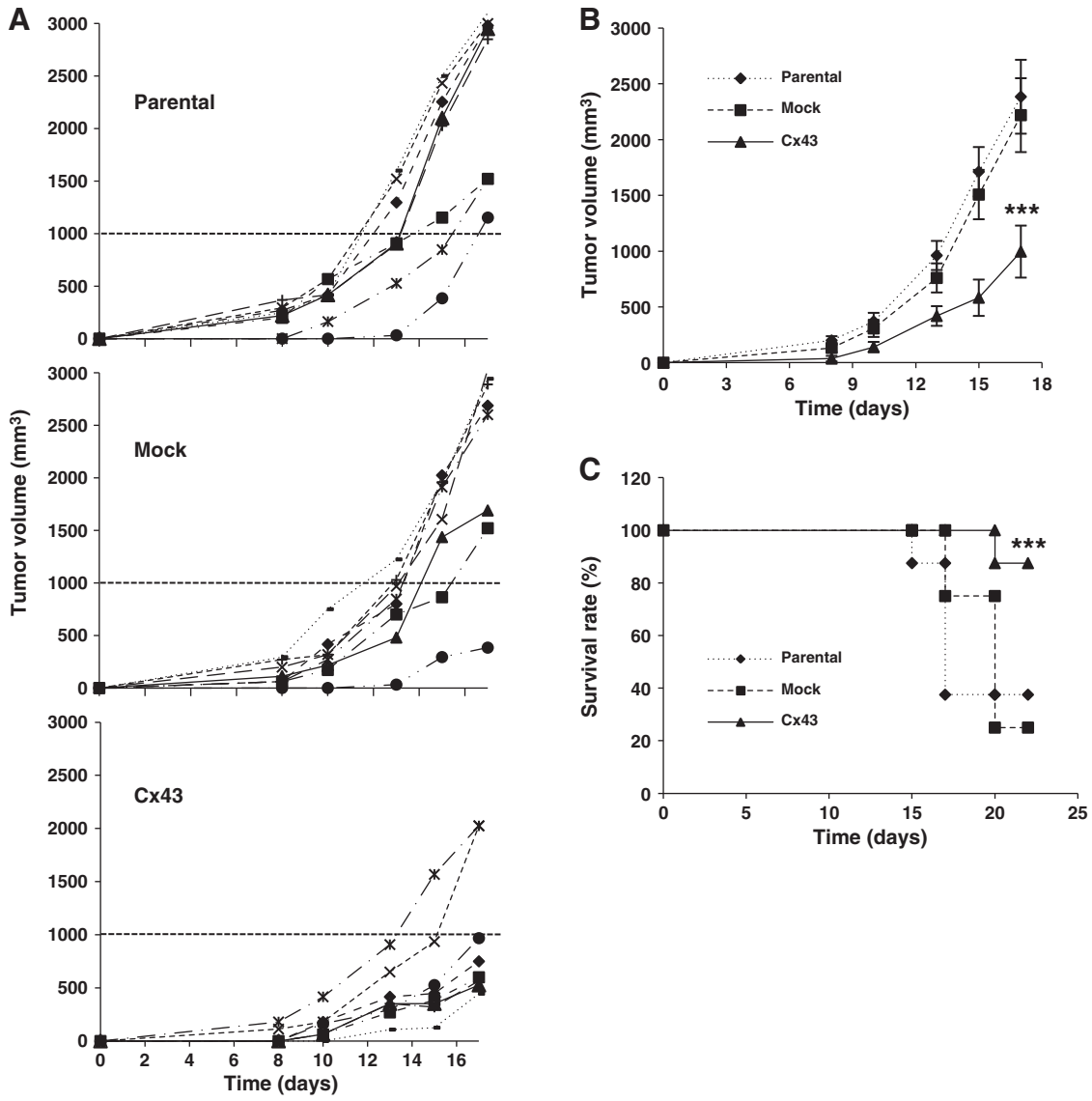

Fig. 4. Overexpression of Cx43 inhibits tumor growth in ES and improves animal survival. Intramuscular paratibial injections of $2 \cdot 10^6$ TC71 tumor cells were performed in 3 groups of 8 nude mice: parental, mock or Cx43-overexpressing. The results are representative for 2 independent experiments (mean ± SEM; ***$p<0.05$). (A) Evolution of tumor volumes of individual animal. (B) Mean tumor volume of each group. (C) Overall survival rates for the 3 groups over a 22-day period.

associated marked decrease of Rb phosphorylation, consistent with the observed blockade of the cell cycle in G0/G1 phase. Similar results were obtained with A673 model (Fig. 5D).

Together these results demonstrated that Cx43 regulates Ewing's tumor growth via modulation of cell proliferation.

3.4. Overexpression of Cx43 in TC71 and A673 ES cells inhibits bone resorption

Since ES altered bone remodeling plays a central role in the development and progression of ES bone tumors, we evaluated the ability of Cx43 to alter tumor-induced bone resorption. To this aim, the microarchitecture of bone was examined after animal sacrifice using a high-resolution X-ray micro-CT system. Analysis of the tibiae/fibulae suggests that Cx43 overexpression decreased tumor-induced bone osteolysis in A673 ES model and favors the bone formation in TC71 ES model. To confirm this observation, the bone volumes were measured after three-dimensional reconstruction (Fig. 6A and B). The mean of bone volumes were 12.5 ± 0.6 mm^3 and 12.7 ± 0.5 mm^3 in mice injected with parental or mock-transfected TC71 cells, respectively, whereas the mean bone volume in mice carrying Cx43–TC71 tumors was 15 ± 0.3 mm^3 (mean ± SEM;***$p<0.01$; Fig. 6A). Similarly, Cx43 enhanced bone volume in mice injected with A673 cells (**$p<0.05$; Fig. 6B). To fully evaluate the ability of Cx43 to increase bone volume, these measures were compared for equivalent tumor volumes at, respectively, 500, 1000 and 3000 mm^3. At a tumor volume of 3000 mm^3, the mean bone volume was 13.3 ± 0.6 mm^3 in mice injected with mock-transfected TC71 cells, compared to 16.4 ± 0.5 mm^3 in mice injected with Cx43-transfected cells (mean ± SEM;***$p<0.01$; Fig. 6C). Furthermore, while bone volumes of control mice remained constant (around 13 mm^3), the bone volumes of mice injected with Cx43-transfected TC71 cells gradually increased with tumor size (from 14.4 ± 0.7 mm^3 to 16.4 ± 0.5 mm^3 when tumor volumes increased from 500 to 3000 mm^3, Fig. 6C). Similar results were obtained with mice injected with A673 ES cells (Supplementary Fig. S3).

To understand the mechanisms underlying the effect of Cx43 on tumor-induced bone formation, the activity of osteoclasts and osteoblasts, two cell lineages implicated in bone remodeling, was assessed. Tartrate resistant acid phosphatase (TRAP) staining in sections of

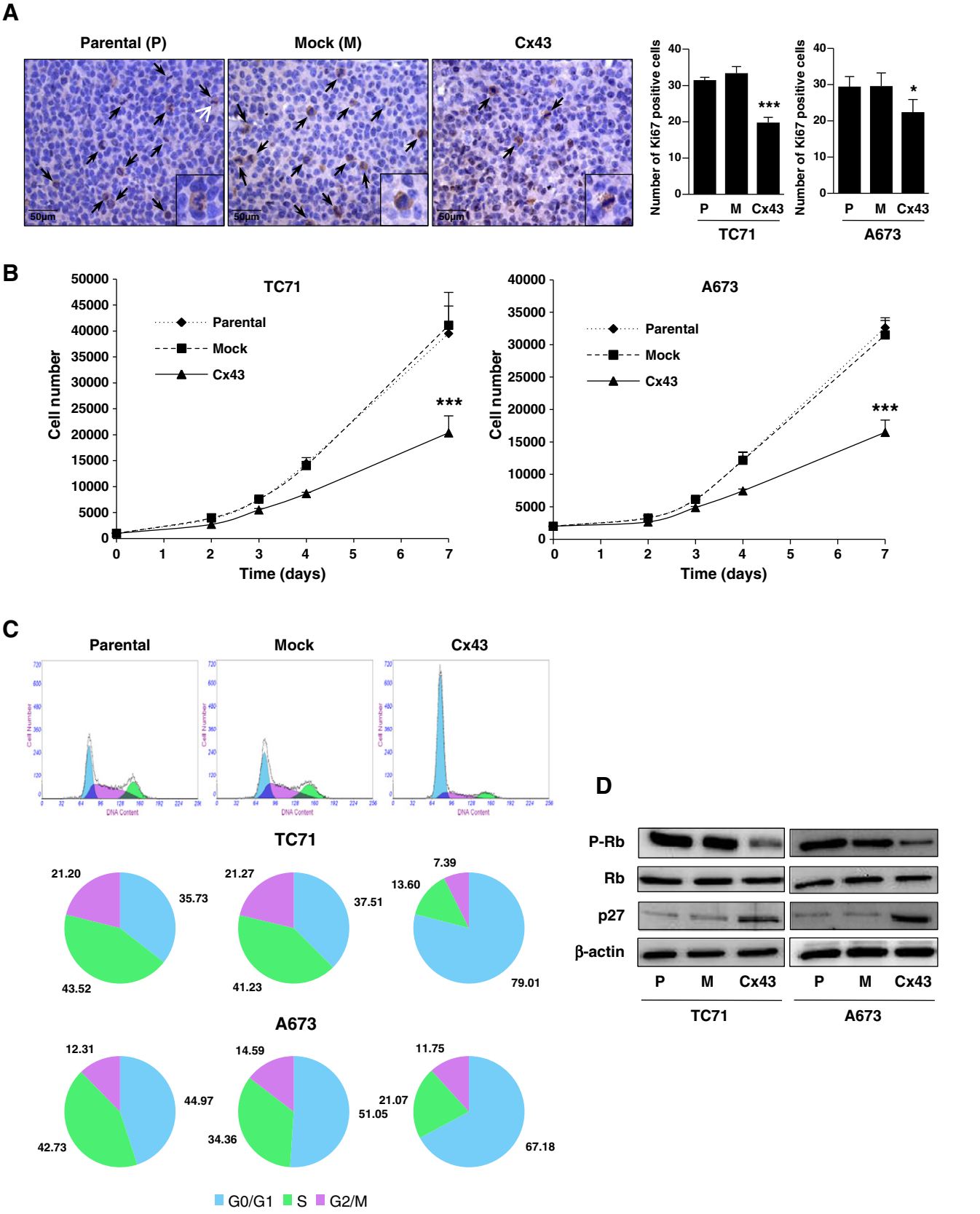

Fig. 5. Overexpression of Cx43 inhibits tumor cell proliferation in ES by a cell cycle arrest in G0/G1 phase. (A) Tumor samples (volume = 3000 mm^3) of each group were fixed, included, sectioned and immunostained with anti-human Ki-67. One representative photomicrograph per group in TC71 ES model was shown for immunostaining Ki-67 (magnification ×40). Ki-67 positive tumor cells (in brown and indicated by arrows) were quantified by manual counting in six random fields microscopy (magnification ×20) in 3 animals per group of each ES experimental model. Histograms represent the mean number of Ki-67 positive cells counted by field (mean ± SEM; *$p<0.05$, ***$p<0.01$). (B) Proliferation assays were performed by cell counting with Trypan Blue to compare the cell proliferation rate between the group overexpressing Cx43 and control groups (parental and mock) (mean ± SD; ***$p<0.01$). (C) After 24 h of culture growth, cell cycle distribution of parental, mock- and Cx43-transfected TC71 (upper and middle panels) and A673 (lower panel) cells was analyzed by propidium iodide staining and flow cytometry. (D) The expression of cell cycle proteins was analyzed by Western blot. Results shown (B, C and D) are representative of 3 independent experiments performed in duplicate.

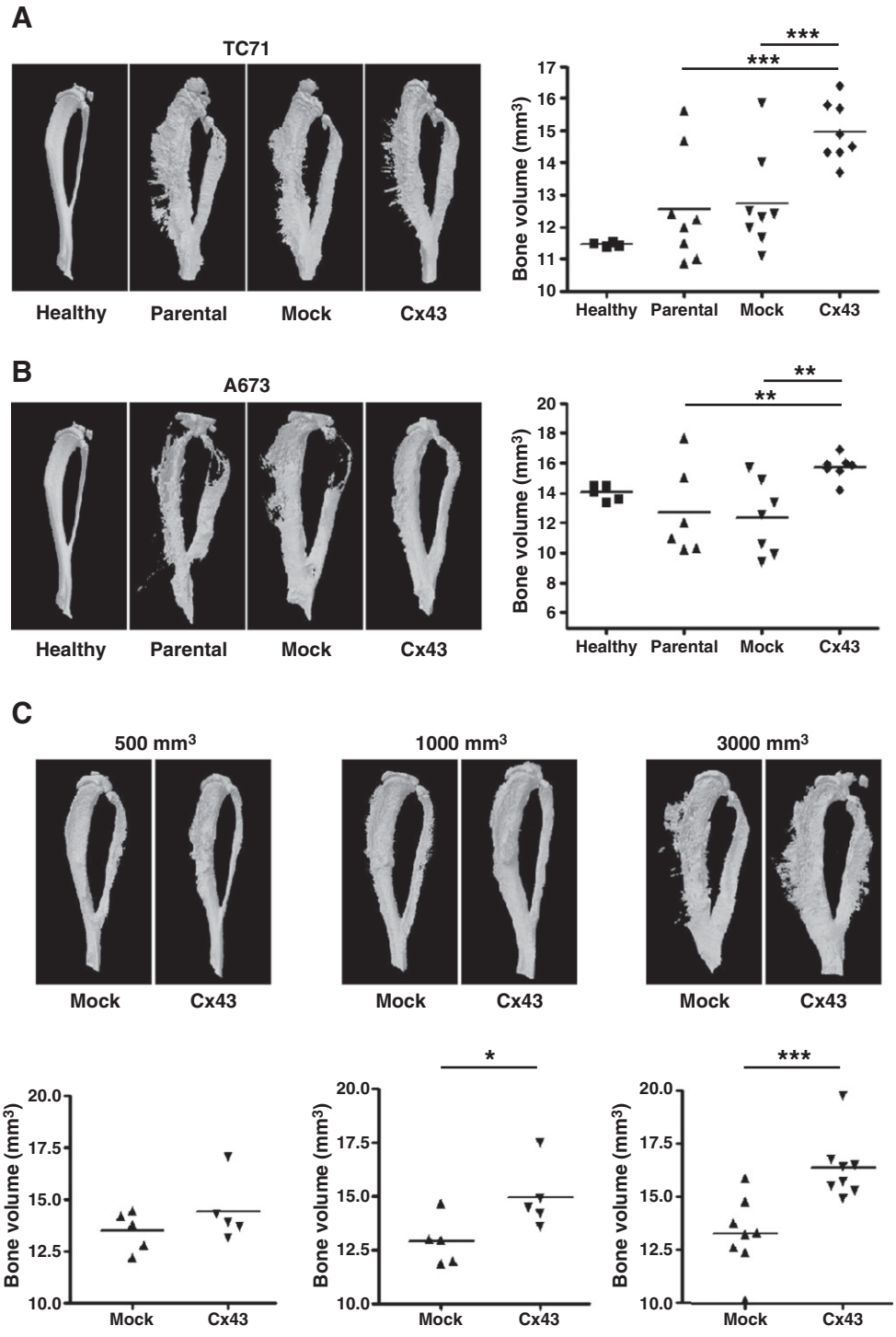

Fig. 6. Overexpression of Cx43 in tumor cells favors bone formation. Intramuscular paratibial injections of TC71 or A673 tumor cells were performed in 3 groups of 8 nude mice: parental, mock or Cx43-overexpressing. These results are representative for 2 independent experiments in each ES experimental model. (A) 3D reconstructions of one representative tibia/fibula (left panel) of each group of TC71 ES model (parental, mock and Cx43-overexpressing) were performed at day 17, and compared to healthy group corresponding to mice bearing no tumors. Tumor volumes in the control group are around 3000 mm^3 whereas the tumor volume in the Cx43-overexpressing group is around 1500 mm^3. Graphs (right panel) represent the bone volume of each animal per group at day 17 (***$p<0.01$). (B) 3D reconstructions of one representative tibia/fibula (left panel) of each group in the A673 ES model were performed at day 21, as shown in Fig. 6A. Graphs (right panel) represent the bone volume of each animal per group at day 21 (**$p<0.05$). (C) 3D reconstructions of tibiae/fibulae (top panel) and bone volume (bottom panel) of animals in the Cx43-overexpressing group compared to mock group in the TC71 model, at the same tumor volumes: 500 mm^3 (left panel), 1000 mm^3 (middle panel) and 3000 mm^3 (right panel) (mean; *$p<0.05$, ***$p<0.01$).

tumor-bearing tibiae showed that Cx43–TC71 tumor cells reduced the number and size of TRAP + multinucleated cells, both in growth plate (Fig. 7A) and at the interface bone-tumor (Fig. 7B), relative to the control conditions. By contrast, osterix immunostaining of the same samples showed no significant difference between mice injected with Cx43-transfected cells and animals receiving parental or mock-transfected cells (Fig. 7C). Similar results were obtained in the A673 model (data not shown).

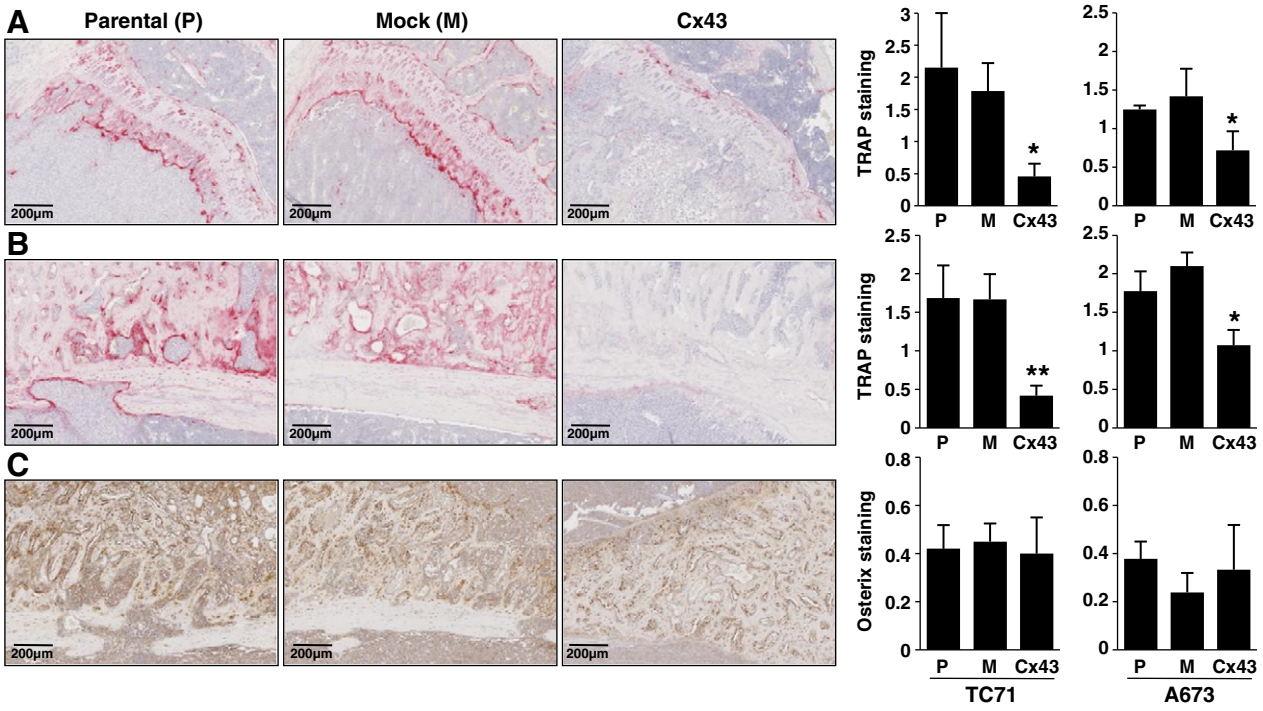

Fig. 7. Overexpression of Cx43 inhibits osteolysis associated with tumor growth of ES. Tumor samples (volume = 3000 mm^3) of each group were fixed, embedded in paraffin, sectioned and stained with TRAP or osterix. One representative photomicrograph per group for TC71 ES mice was shown for TRAP and osterix staining (magnification ×10). For TRAP staining, positives osteoclasts were quantified using ImageJ software. Results are expressed as the percentage of osteoclast surface. Histograms represent the mean of positive staining ± SEM of 2 independent experiments (n = 8 per group) in each ES experimental model (*$p<0.05$, **$p<0.01$). (A) TRAP staining was performed to identify osteoclast activity at the level of the growth plate. (B) TRAP staining was performed to identify osteoclast activity at the interface between tumor and cortical bone at the level of ectopic bone neoformation. (C) Osterix immunostaining was performed to identify osteoblasts at the interface between tumor and cortical bone at the level of ectopic bone neoformation.

Taken together, our results demonstrated that Cx43-induced bone formation may be due to inhibition of osteoclast activity rather than to a stimulation of osteoblast activity.

4. Discussion

Observations indicating a role of connexin in tumorigenesis are supported by many in vitro analyses demonstrating the down-regulation or loss of connexin expression in a wide range of neoplastic cells and primary tumors [35–37]. Here, we demonstrated a loss of Cx43 gene expression in ES cell lines. Early works using the NIH3T3 cell model have demonstrated that EWS–FLI1 acts as a transcriptional activator that allows oncogenic transformation [38,39]. Current opinion holds that EWS–FLI1 functions as an aberrant transcription factor supported by works which demonstrated that EWS–FLI1 localizes to the nucleus, binds DNA in a site-specific manner and possesses a powerful transcriptional activator that is more potent than the native FLI1 [7]. Gene expression studies have further demonstrated that EWS–FLI1 is able to enhance the expression of many genes implicated in transformation and/or tumor progression, including MYC [40], ID2 [41], CCND1 [42] and PDGFC [43]. Other studies have revealed that EWS–FLI1 is able to decrease the expression of many genes including those encoding p21 [44], p57kip [45], TGFβRII [46] and IGFBP3 [47]. Among these, only the TGFβRII and IGFBP3 genes, which are down-regulated by EWS–FLI1, have been identified as direct EWS–FLI1 targets [48]. Here, using a EWS–FLI1 knock-down approach, we demonstrated that EWS–FLI1 affects the Cx43 gene expression, suggesting that Cx43 is a EWS–FLI1 target gene. However, we cannot exclude that Cx43 induction in response to EWS–FLI1 silencing is a consequence of modified cell differentiation for example. The exact mechanisms underlying the down-regulation of Cx43 gene by EWS–FLI1 remain to be elucidated.

Through a molecular gain-of-function approach, we demonstrated that Cx43 overexpression inhibits in vivo ES tumor growth, providing the first experimental evidence indicating that the decrease of Cx43 gene expression is one mechanism through which ES cells can acquire high tumor growth potential. Since the main function of connexins is the formation of intercellular channels, the mechanisms by which connexins modulate cell proliferation and thus tumor growth were firstly proposed to depend on the ability of these channels to promote exchange of molecules that regulate the cell cycle [49]. Over the past 40 years, numerous studies have demonstrated a loss or at least a decrease of GJIC between cancer cells or between cancer cells and their surrounding normal cells, supporting the link between gap junction defects and tumor growth [20]. In agreement with this dogma, numerous studies reported that many tumor promoters were indeed inhibitors of GJIC [50] supporting the idea that the inhibition of GJIC during the tumor promoting stage may favor the clonal expansion of initiated cells [20,51]. It was thus proposed that the recovery of GJIC between cancer cells could inhibit their proliferation and by consequence in vivo tumor growth. In this context, over-expression of connexins in different tumor cells was shown to restore GJIC and therefore inhibit cell proliferation [20,21,35]. Although we showed that Cx43 overexpression in ES cells restores GJIC, we cannot exclude that the effect of Cx43 overexpression on cell proliferation and in vivo tumor growth was not associated with the restoration of GJIC. Indeed, numerous studies have provided evidence for a dissociation of GJIC and the ability of connexins to inhibit cell proliferation and tumor growth [21]. Mechanistic studies demonstrated that Cx43 overexpression may inhibit cell proliferation via the inhibition of the expression of S phase kinase associated protein 2 (skp2), the protein that promotes the ubiquitination of cyclin-dependent kinase inhibitor p27kip [49]. With regard to primary bone tumors, a down-regulation of cyclin D1 associated with a blockade of the cell cycle in G0/G1

phase was observed in osteosarcoma after Cx43 overexpression [52]. Supporting this observation, we demonstrated that Cx43 overexpression in ES cells increases p27 levels with an associated marked decrease of Rb phosphorylation, consistent with the observed blockade of the cell cycle in G0/G1 phase.

The presence of a "vicious cycle" established between tumor proliferation and paratumor osteolysis plays a crucial role in the development of primary bone tumors [53]. Cancer cells produce soluble factors that activate directly or indirectly via osteoblasts, osteoclast differentiation and maturation [54,55]. In turn, during bone degradation, osteoclasts release tumor supportive growth factors stocked in the mineralized bone matrix [56]. Studies about the cellular mechanisms underlying the rapid bone resorption in ES indicate that ES cells activate osteoclast activity [4]. According with these findings, we demonstrated that the increase in bone volume observed after Cx43 overexpression in ES cells is due in large part to inhibition of osteoclast activity rather than to stimulation of osteoblast activity. The decrease of TRAP activity at the level of the growth plate, that is, not in direct contact with the tumor, suggests that the overexpression of Cx43 affects the ability of the tumor cells to produce a soluble factor able to regulate osteoclast activity, such as RANKL or M-CSF. This hypothesis is supported by previous reports demonstrating that ES cells support osteoclast formation by a RANKL- and M-CSF-dependent mechanism [4].

In conclusion, this report provides new insights regarding the role of the tumor suppressor gene Cx43 in the first stage of ES development, specifically during the primary bone tumor growth. We specifically demonstrated: 1) that Cx43 gene expression affects tumor growth by a blockade of the cell cycle in G0/G1 phase consistent with an increase of p27 level, and 2) that Cx43 gene expression plays a crucial role in the "vicious cycle" established between tumor proliferation and paratumor osteolysis by its ability to decrease osteoclast activity. The role of Cx43 in the more late stage of ES development like metastatic dissemination remains to be elucidated. Indeed, the role of connexins in invasion and metastasis seems to be even more complex, and several reports suggest that connexins might facilitate invasion, intravasation, extravasation and metastasis [57].

Supplementary data to this article can be found online at http://dx.doi.org/10.1016/j.bbadis.2013.01.001.

Acknowledgements

We thank Steven Nedellec and Philippe Hulin for their technical assistance (Plateau d'imagerie cellulaire - PICell, SFR Bonamy, FED 4203/Inserm UMS 016/CNRS 3556, Nantes France).

Conflict of interest

The authors declare no conflict of interest.

References

[1] A. Bleyer, R. Barr, B. Hayes-Lattin, D. Thomas, C. Ellis, B. Anderson, The distinctive biology of cancer in adolescents and young adults, Nat. Rev. Cancer 8 (2008) 288–298.
[2] N.J. Balamuth, R.B. Womer, Ewing's sarcoma, Lancet Oncol. 11 (2010) 184–192.
[3] P. Jedlicka, Ewing sarcoma, an enigmatic malignancy of likely progenitor cell origin, driven by transcription factor oncogenic fusions, Int. J. Clin. Exp. Pathol. 3 (2010) 338–347.
[4] R. Taylor, H.J. Knowles, N.A. Athanasou, Ewing sarcoma cells express RANKL and support osteoclastogenesis, J. Pathol. 225 (2011) 195–202.
[5] C. Turc-Carel, A. Aurias, F. Mugneret, S. Lizard, I. Sidaner, C. Volk, J.P. Thiery, S. Olschwang, I. Philip, M.P. Berger, Chromosomes in Ewing's sarcoma I. An evaluation of 85 cases of remarkable consistency of t(11;22)(q24;q12), Cancer Genet. Cytogenet. 32 (1988) 229–238.
[6] O. Delattre, J. Zucman, B. Plougastel, C. Desmaze, T. Melot, M. Peter, H. Kovar, I. Joubert, P. de Jong, G. Rouleau, Gene fusion with an ETS DNA-binding domain caused by chromosome translocation in human tumours, Nature 359 (1992) 162–165.
[7] N. Riggi, I. Stamenkovic, The biology of Ewing sarcoma, Cancer Lett. 254 (2007) 1–10.
[8] F. Tirode, K. Laud-Duval, A. Prieur, B. Delorme, P. Charbord, O. Delattre, Mesenchymal stem cell features of Ewing tumors, Cancer Cell 11 (2007) 421–429.
[9] G.E. Sosinsky, B.J. Nicholson, Structural organization of gap junction channels, Biochim. Biophys. Acta 1711 (2005) 99–125.
[10] N.M. Kumar, N.B. Gilula, The gap junction communication channel, Cell 84 (1996) 381–388.
[11] C. Tacheau, J. Fontaine, J. Loy, A. Mauviel, F. Verrecchia, TGF-beta induces connexin43 gene expression in normal murine mammary gland epithelial cells via activation of p38 and PI3K/AKT signaling pathways, J. Cell. Physiol. 217 (2008) 759–768.
[12] C. Tacheau, J. Laboureau, A. Mauviel, F. Verrecchia, TNF-alpha represses connexin43 expression in HaCat keratinocytes via activation of JNK signaling, J. Cell. Physiol. 216 (2008) 438–444.
[13] F. Verrecchia, F. Duthe, S. Duval, I. Duchatelle, D. Sarrouilhe, J.C. Herve, ATP counteracts the rundown of gap junctional channels of rat ventricular myocytes by promoting protein phosphorylation, J. Physiol. (Lond.) 516 (Pt 2) (1999) 447–459.
[14] F. Verrecchia, J. Hervé, Reversible inhibition of gap junctional communication by tamoxifen in cultured cardiac myocytes, Pflugers Arch. 434 (1997) 113–116.
[15] F. Pluciennik, F. Verrecchia, B. Bastide, J.C. Hervé, M. Joffre, J. Délèze, Reversible interruption of gap junctional communication by testosterone propionate in cultured Sertoli cells and cardiac myocytes, J. Membr. Biol. 149 (1996) 169–177.
[16] S.-S. Zhang, R.M. Shaw, Multilayered regulation of cardiac ion channels, Biochim. Biophys. Acta (in press), http://dx.doi.org/10.1016/j.bbamcr.2012.10.020.
[17] G.L. Firestone, B.J. Kapadia, Minireview: regulation of gap junction dynamics by nuclear hormone receptors and their ligands, Mol. Endocrinol. 26 (2012) 1798–1807.
[18] L. Matsuuchi, C.C. Naus, Gap junction proteins on the move: connexins, the cytoskeleton and migration, Biochim. Biophys. Acta 1828 (2013) 94–108.
[19] C.C.G. Naus, Gap junctions and tumour progression, Can. J. Physiol. Pharmacol. 80 (2002) 136–141.
[20] M. Mesnil, S. Crespin, J.-L. Avanzo, M.-L. Zaidan-Dagli, Defective gap junctional intercellular communication in the carcinogenic process, Biochim. Biophys. Acta 1719 (2005) 125–145.
[21] L. Cronier, S. Crespin, P.-O. Strale, N. Defamie, M. Mesnil, Gap junctions and cancer: new functions for an old story, Antioxid. Redox Signal. 11 (2009) 323–338.
[22] V.A. Krutovskikh, S.M. Troyanovsky, C. Piccoli, H. Tsuda, M. Asamoto, H. Yamasaki, Differential effect of subcellular localization of communication impairing gap junction protein connexin43 on tumor cell growth in vivo, Oncogene 19 (2000) 505–513.
[23] M. Momiyama, Y. Omori, Y. Ishizaki, Y. Nishikawa, T. Tokairin, J. Ogawa, K. Enomoto, Connexin26-mediated gap junctional communication reverses the malignant phenotype of MCF-7 breast cancer cells, Cancer Sci. 94 (2003) 501–507.
[24] D.A. Goodenough, D.L. Paul, Beyond the gap: functions of unpaired connexon channels, Nat. Rev. Mol. Cell Biol. 4 (2003) 285–294.
[25] P.J. Kausalya, D.C.Y. Phua, W. Hunziker, Association of ARVCF with zonula occludens (ZO)-1 and ZO-2: binding to PDZ-domain proteins and cell–cell adhesion regulate plasma membrane and nuclear localization of ARVCF, Mol. Biol. Cell 15 (2004) 5503–5515.
[26] B.N.G. Giepmans, Gap junctions and connexin-interacting proteins, Cardiovasc. Res. 62 (2004) 233–245.
[27] R. Civitelli, Cell–cell communication in the osteoblast/osteocyte lineage, Arch. Biochem. Biophys. 473 (2008) 188–192.
[28] S.A. Bustin, Why the need for qPCR publication guidelines? — The case for MIQE, Methods 50 (2010) 217–226.
[29] J.R. De Leon, P.M. Buttrick, G.I. Fishman, Functional analysis of the connexin43 gene promoter in vivo and in vitro, J. Mol. Cell. Cardiol. 26 (1994) 379–389.
[30] K. Kimura, S. Teranishi, T. Nishida, Establishment of human corneal epithelial cells stably expressing human connexin43, Exp. Eye Res. 90 (2010) 4–9.
[31] G.S. Goldberg, J.F. Bechberger, C.C. Naus, A pre-loading method of evaluating gap junctional communication by fluorescent dye transfer, Biotechniques 18 (1995) 490–497.
[32] K. Ziambaras, F. Lecanda, T.H. Steinberg, R. Civitelli, Cyclic stretch enhances gap junctional communication between osteoblastic cells, J. Bone Miner. Res. 13 (1998) 218–228.
[33] D. Heymann, B. Ory, F. Blanchard, M.-F. Heymann, P. Coipeau, C. Charrier, S. Couillaud, J.P. Thiery, F. Gouin, F. Redini, Enhanced tumor regression and tissue repair when zoledronic acid is combined with ifosfamide in rat osteosarcoma, Bone 37 (2005) 74–86.
[34] V. Valiunas, S. Doronin, L. Valiuniene, I. Potapova, J. Zuckerman, B. Walcott, R.B. Robinson, M.R. Rosen, P.R. Brink, I.S. Cohen, Human mesenchymal stem cells make cardiac connexins and form functional gap junctions, J. Physiol. (Lond.) 555 (2004) 617–626.
[35] C.C. Naus, J.F. Bechberger, S. Caveney, J.X. Wilson, Expression of gap junction genes in astrocytes and C6 glioma cells, Neurosci. Lett. 126 (1991) 33–36.
[36] S. Jamieson, J.J. Going, R. D'Arcy, W.D. George, Expression of gap junction proteins connexin 26 and connexin 43 in normal human breast and in breast tumours, J. Pathol. 184 (1998) 37–43.
[37] M.M. Saunders, M.J. Seraj, Z. Li, Z. Zhou, C.R. Winter, D.R. Welch, H.J. Donahue, Breast cancer metastatic potential correlates with a breakdown in homospecific and heterospecific gap junctional intercellular communication, Cancer Res. 61 (2001) 1765–1767.
[38] W.A. May, M.L. Gishizky, S.L. Lessnick, L.B. Lunsford, B.C. Lewis, O. Delattre, J. Zucman, G. Thomas, C.T. Denny, Ewing sarcoma 11;22 translocation produces a chimeric transcription factor that requires the DNA-binding domain encoded by FLI1 for transformation, Proc. Natl. Acad. Sci. U. S. A. 90 (1993) 5752–5756.

[39] S.L. Lessnick, B.S. Braun, C.T. Denny, W.A. May, Multiple domains mediate transformation by the Ewing's sarcoma EWS/FLI-1 fusion gene, Oncogene 10 (1995) 423–431.
[40] R.A. Bailly, R. Bosselut, J. Zucman, F. Cormier, O. Delattre, M. Roussel, G. Thomas, J. Ghysdael, DNA-binding and transcriptional activation properties of the EWS–FLI-1 fusion protein resulting from the t(11;22) translocation in Ewing sarcoma, Mol. Cell. Biol. 14 (1994) 3230–3241.
[41] M. Fukuma, H. Okita, J.-I. Hata, A. Umezawa, Upregulation of Id2, an oncogenic helix–loop–helix protein, is mediated by the chimeric EWS/ets protein in Ewing sarcoma, Oncogene 22 (2003) 1–9.
[42] D.H. Wai, K.-L. Schaefer, A. Schramm, E. Korsching, F. Van Valen, T. Ozaki, W. Boecker, L. Schweigerer, B. Dockhorn-Dworniczak, C. Poremba, Expression analysis of pediatric solid tumor cell lines using oligonucleotide microarrays, Int. J. Oncol. 20 (2002) 441–451.
[43] J.P. Zwerner, W.A. May, PDGF-C is an EWS/FLI induced transforming growth factor in Ewing family tumors, Oncogene 20 (2001) 626–633.
[44] F. Nakatani, K. Tanaka, R. Sakimura, Y. Matsumoto, T. Matsunobu, X. Li, M. Hanada, T. Okada, Y. Iwamoto, Identification of p21WAF1/CIP1 as a direct target of EWS–Fli1 oncogenic fusion protein, J. Biol. Chem. 278 (2003) 15105–15115.
[45] L. Dauphinot, C. De Oliveira, T. Melot, N. Sevenet, V. Thomas, B.E. Weissman, O. Delattre, Analysis of the expression of cell cycle regulators in Ewing cell lines: EWS–FLI-1 modulates p57KIP2and c-Myc expression, Oncogene 20 (2001) 3258–3265.
[46] K.B. Hahm, K. Cho, C. Lee, Y.H. Im, J. Chang, S.G. Choi, P.H. Sorensen, C.J. Thiele, S.J. Kim, Repression of the gene encoding the TGF-beta type II receptor is a major target of the EWS–FLI1 oncoprotein, Nat. Genet. 23 (1999) 222–227.
[47] A. Prieur, F. Tirode, P. Cohen, O. Delattre, EWS/FLI-1 silencing and gene profiling of Ewing cells reveal downstream oncogenic pathways and a crucial role for repression of insulin-like growth factor binding protein 3, Mol. Cell. Biol. 24 (2004) 7275–7283.
[48] S.L. Lessnick, M. Ladanyi, Molecular pathogenesis of ewing sarcoma: new therapeutic and transcriptional targets, Annu. Rev. Pathol. 7 (2012) 145–159.
[49] J. Czyz, The stage-specific function of gap junctions during tumourigenesis, Cell. Mol. Biol. Lett. 13 (2008) 92–102.
[50] I.V. Budunova, G.M. Williams, Cell culture assays for chemicals with tumor-promoting or tumor-inhibiting activity based on the modulation of intercellular communication, Cell Biol. Toxicol. 10 (1994) 71–116.
[51] M. Mesnil, H. Yamasaki, Cell–cell communication and growth control of normal and cancer cells: evidence and hypothesis, Mol. Carcinog. 7 (1993) 14–17.
[52] Y.W. Zhang, I. Morita, M. Ikeda, K.W. Ma, S. Murota, Connexin43 suppresses proliferation of osteosarcoma U2OS cells through post-transcriptional regulation of p27, Oncogene 20 (2001) 4138–4149.
[53] K.G. Halvorson, M.A. Sevcik, J.R. Ghilardi, T.J. Rosol, P.W. Mantyh, Similarities and differences in tumor growth, skeletal remodeling and pain in an osteolytic and osteoblastic model of bone cancer, Clin. J. Pain 22 (2006) 587–600.
[54] M. Grano, G. Mori, V. Minielli, F.P. Cantatore, S. Colucci, A.Z. Zallone, Breast cancer cell line MDA-231 stimulates osteoclastogenesis and bone resorption in human osteoclasts, Biochem. Biophys. Res. Commun. 270 (2000) 1097–1100.
[55] T.A. Guise, J.J. Yin, S.D. Taylor, Y. Kumagai, M. Dallas, B.F. Boyce, T. Yoneda, G.R. Mundy, Evidence for a causal role of parathyroid hormone-related protein in the pathogenesis of human breast cancer-mediated osteolysis, J. Clin. Invest. 98 (1996) 1544–1549.
[56] J. Pfeilschifter, G.R. Mundy, Modulation of type beta transforming growth factor activity in bone cultures by osteotropic hormones, Proc. Natl. Acad. Sci. U. S. A. 84 (1987) 2024–2028.
[57] C.C. Naus, D.W. Laird, Implications and challenges of connexin connections to cancer, Nat. Rev. Cancer 10 (2010) 435–441.